# Lab 4: Numerical Solutions of Elliptic and Nonlinear PDEs Using Gauss-Seidel, FTCS, and Leapfrog Methods

Umi Yamaguchi
November 17, 2024

## Background

This lab explores numerical methods for solving partial differential equations (PDEs) that are fundamental in physics, such as Laplace's equation, Burger's equation, and the shallow water equations. These equations model a range of physical phenomena, including electrostatic potentials in empty space, nonlinear wave propagation, and fluid dynamics in shallow bodies of water. We will utilize computational techniques like the Gauss-Seidel iterative method and the leapfrog method to investigate these equations, employing Python for efficient computation and visualization.

Numerical solutions of PDEs pose significant computational challenges, particularly regarding stability and accuracy. Methods like the Forward-Time Centered-Space (FTCS) scheme, while straightforward, can be unstable for certain types of equations, leading to divergent or non-physical solutions. To overcome these challenges, we will implement over-relaxation in the Gauss-Seidel method to accelerate convergence and use the leapfrog method to enhance stability in time-dependent simulations.

In this lab, we will compute the electrostatic potential within a capacitor setup using the Gauss-Seidel method, both with and without over-relaxation, and visualize the resulting electric field lines using stream plots. For the shallow water equations, we will reformulate them into flux-conservative form and apply the FTCS scheme to simulate wave propagation, observing any stability issues that arise. Lastly, we will employ the leapfrog method to solve Burger's equation, analyzing the evolution of nonlinear waves and addressing the numerical instabilities associated with such simulations.

# 1. Electrostatics and Laplace's Equation

We begin our investigation by exploring the numerical solution of Laplace's equation in the context of electrostatics. Laplace's equation, $\nabla^2 V = 0$, describes the behavior of the electrostatic potential $V(x, y)$ in regions without charge. Solving this equation with appropriate boundary conditions allows us to determine the electric potential and, consequently, the electric field $\mathbf{E} = -\nabla V$ within the domain.

In this experiment, we consider a simplified two-dimensional model of an electronic capacitor consisting of two flat metal plates enclosed in a square metal box (Figure 1).

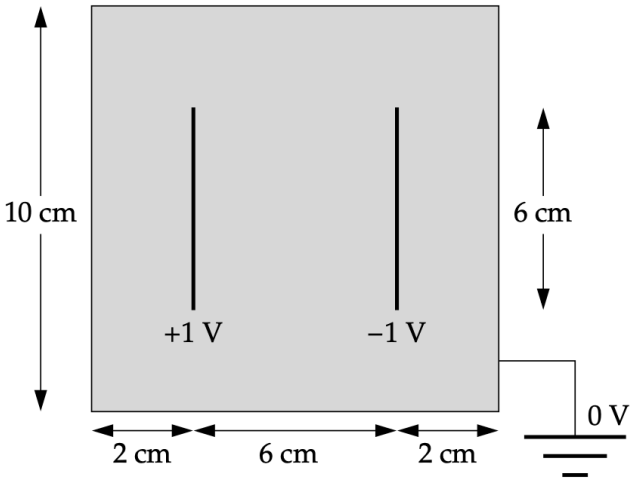


Figure 1: Capacitor for Question 1 (from Newman, p.417).

The walls of the box are held at zero potential, while the two plates are maintained at potentials of $\pm 1\,\mathrm{V}$. We will use the Gauss-Seidel method without over-relaxation to numerically compute the potential at each point on a $100 \times 100$ grid, iterating until a precision of $10^{-6}\,\mathrm{V}$ is achieved at each grid point.

The Gauss-Seidel update formula for Laplace's equation is:

$V_{i,j} = \frac{1}{4}\left(V_{i+1,j} + V_{i-1,j} + V_{i,j+1} + V_{i,j-1}\right)$, where $V_{i,j}$ is the potential at grid point $(i, j)$.

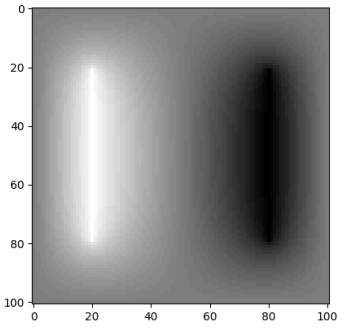


Figure 2: Contour plot of the electrostatic potential for a parallel-plate capacitor, showing symmetric potential distribution and steep gradients near the plates within a grounded box.

The contour plot of the electrostatic potential $V(x, y)$ inside the $100 \times 100$ grid illustrates the solution to Laplace's equation for the modeled parallel-plate capacitor. The symmetry of the potential field is evident, reflecting the equal and opposite charges on the plates. This plot shows the application of the Gauss-Seidel method to solve for the potential under specified boundary conditions.

We will also explore the effect of over-relaxation by introducing a relaxation parameter $\omega$ in the Gauss-Seidel update formula:

$$V_{i,j} \leftarrow (1+\omega)\frac{1}{4}\left(V_{i+1,j} + V_{i-1,j} + V_{i,j+1} + V_{i,j-1}\right) - \omega V_{i,j}, \text{ where } 0 < \omega < 1.$$

By experimenting with different values of $\omega$, we aim to observe the impact on convergence speed and solution accuracy.

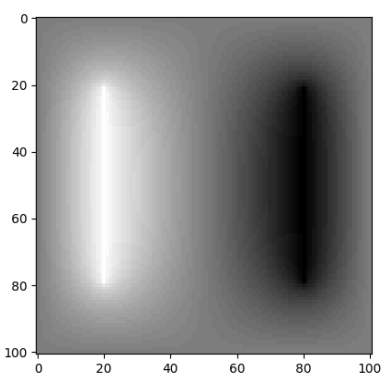


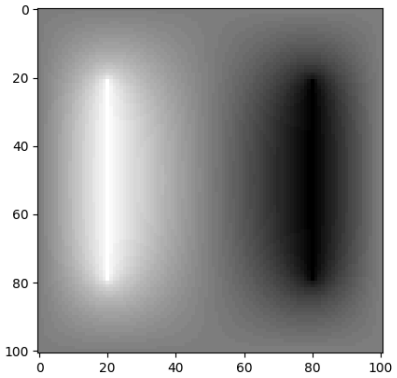


Figure 3 and 4: Contour plot of the electrostatic potential for a parallel-plate capacitor with $\omega = 0.1$ and $\omega = 0.5$ which appear identical.

By implementing the Gauss-Seidel method with over-relaxation for $\omega = 0.1$ and $\omega = 0.5$, we observed that the resulting potential plots are virtually identical. This is because the relaxation parameter $\omega$ affects the convergence rate of the iterative method but does not alter the final solution of Laplace's equation. The over-relaxation technique accelerates the convergence toward the steady-state solution by adjusting how new estimates incorporate residual errors, but once convergence is achieved to the specified precision, the computed potentials should be the same regardless of the $\omega$ value used.

The similarity in the plots indicates that both $\omega = 0.1$ and $\omega = 0.5$ led the algorithm to the same electrostatic potential distribution that satisfies the boundary conditions of the problem. While higher $\omega$ values generally speed up convergence, they can also introduce instability if too large. In our case, both values were within a suitable range to ensure stable convergence, resulting in identical potential profiles.

Finally, we will visualize the electric field by creating stream plots of the field lines, color-coded by the electric potential. This involves computing the electric field components:

$$E_x = -\frac{\partial V}{\partial x}, \quad E_y = -\frac{\partial V}{\partial y},$$

which can be approximated using finite differences on the computed potential grid.

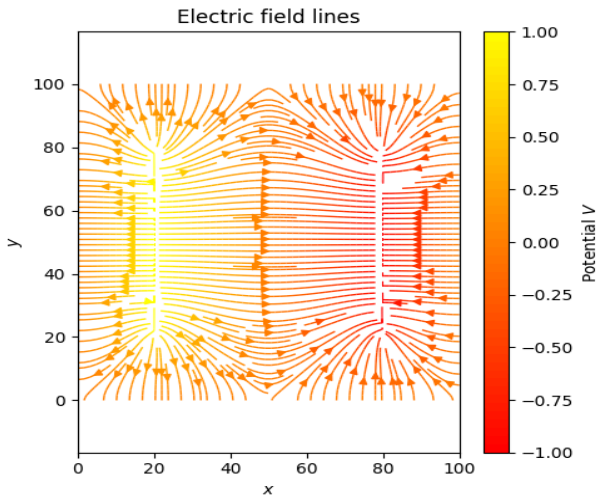


Figure 5: Stream plot of electric field lines for a parallel-plate capacitor, showing field direction from the positively charged plate to the negatively charged plate, with a color gradient representing the electric potential.

The stream plot illustrates the electric field lines derived from the electrostatic potential $V(x, y)$ for the parallel-plate capacitor system. The field lines emerge perpendicular to the plates, moving from the positively charged plate $(+1\,V)$ to the negatively charged plate $(-1\,V)$, consistent with the physics of electric fields. The color gradient along the lines represents the potential, transitioning from yellow near the positive plate to red near the negative plate.

## 2. Shallow Water Equations

Next, we examine fluid dynamics by exploring the shallow water equations, which simplify the Navier-Stokes equations for modeling fluid flow where horizontal dimensions greatly exceed vertical depth. In one dimension, the shallow water equations are:

$$\frac{\partial u}{\partial t} + u\frac{\partial u}{\partial x} = -g\frac{\partial \eta}{\partial x} \quad , \quad \frac{\partial \eta}{\partial t} + \frac{\partial}{\partial x}(uh) = 0 \quad ,$$

where $u(x,t)$ is the horizontal fluid velocity, $\eta(x,t)$ is the free surface elevation, $h = \eta - \eta_b$ is the fluid depth, $\eta_b(x)$ is the bottom topography (assumed constant), $g$ is the acceleration due to gravity. Our goal is to reformulate these equations into flux-conservative form to facilitate numerical solutions using the FTCS scheme. By expressing the equations as:

$$\frac{\partial \vec{u}}{\partial t} = -\frac{\partial \vec{F}(\vec{u})}{\partial x} \quad , \quad \vec{u} = \begin{bmatrix} u \\ \eta \end{bmatrix} , \quad \vec{F}(\vec{u}) = \begin{bmatrix} \frac{1}{2}u^2 + g\eta \\ hu \end{bmatrix}$$

By starting with $\frac{\partial u}{\partial t} + u\frac{\partial u}{\partial x} + g\frac{\partial \eta}{\partial x} = 0$, and $\frac{\partial \eta}{\partial t} + \frac{\partial (u\eta)}{\partial x} = 0$

We first take derivation for $\frac{\partial u}{\partial t}$.

we get $\frac{\partial u}{\partial t} + \frac{\partial}{\partial x}\left(\frac{1}{2}u^2 + g\eta\right) = 0$ Which gives $\frac{\partial u}{\partial t} = -\frac{\partial}{\partial x}\left(\frac{1}{2}u^2 + g\eta\right)$.

Next, we going to take derivation for $\dfrac{\partial \eta}{\partial t}$.

Where it will be $\dfrac{\partial \eta}{\partial t} + \dfrac{\partial}{\partial x}\left(u(\eta - \eta_b)\right) = 0$ which equals to $\dfrac{\partial \eta}{\partial t} = -\dfrac{\partial}{\partial x}\left(u(\eta - \eta_b)\right)$.

From the definition, we can define the system of variables as

$\dfrac{\partial \vec{u}}{\partial t} = \left[\frac{\partial u}{\partial t}, \frac{\partial \eta}{\partial t}\right]$

and as a flux term:

$\dfrac{\partial \vec{F}(\vec{u})}{\partial x} = \left[\frac{\partial}{\partial x}\left(\frac{1}{2}u^2 + g\eta\right), \frac{\partial}{\partial x}\left(u(\eta - \eta_b)\right)\right]$

We can then explicitly show:

$\dfrac{\partial \vec{u}}{\partial t} = -\dfrac{\partial}{\partial x}\left[\frac{1}{2}u^2 + g\eta, u(\eta - \eta_b)\right]$

We then discretize the equations using finite differences. The FTCS scheme approximates the time and space derivatives as:

$$\frac{\partial u}{\partial t} \approx \frac{u_j^{n+1} - u_j^n}{\Delta t}, \frac{\partial F}{\partial x} \approx \frac{F_{j+1}^n - F_{j-1}^n}{2\Delta x},$$

where $n$ and $j$ are the time and space indices, respectively. The update equations become:

$$u_j^{n+1} = u_j^n - \frac{\Delta t}{2\Delta x}\left(F_{u,j+1}^n - F_{u,j-1}^n\right),$$

$$\eta_j^{n+1} = \eta_j^n - \frac{\Delta t}{2\Delta x}\left(F_{\eta,j+1}^n - F_{\eta,j-1}^n\right),$$

where $F_u$ and $F_\eta$ are the components of $\vec{F}$.

Implementing the FTCS scheme, we aim to simulate wave propagation in a shallow fluid under specified initial and boundary conditions, observing how the solution evolves over time. We will also examine numerical instabilities that may arise due to the limitations of the FTCS method.

The shallow water system is modeled on a one-dimensional domain $x \in [0, 1]$ m with 50 spatial grid points $(\Delta x = 0.02)$. The simulation uses a constant time step of $\Delta t = 0.01$ s. The initial condition for the fluid surface elevation $\eta(x, t)$ is given as:

$$\eta(x, 0) = H + Ae^{-\frac{(x-\mu)^2}{\sigma^2}} - \langle Ae^{-\frac{(x-\mu)^2}{\sigma^2}} \rangle,$$

where:

- $H = 0.01\,\mathrm{m}$: the equilibrium water column height,
- $A = 0.002\,\mathrm{m}$: the amplitude of the initial Gaussian disturbance,
- $\mu = 0.5\,\mathrm{m}$: the center of the Gaussian,
- $\sigma = 0.05\,\mathrm{m}$: the width of the Gaussian.

The fluid velocity is initially zero: $u(x, 0) = 0$. We simulate the evolution of $\eta(x, t)$ at three specific times: $t = 0.0\,\mathrm{s}$, $t = 1.0\,\mathrm{s}$, and $t = 4.0\,\mathrm{s}$, and the resulting $\eta(x, t)$ is plotted below.

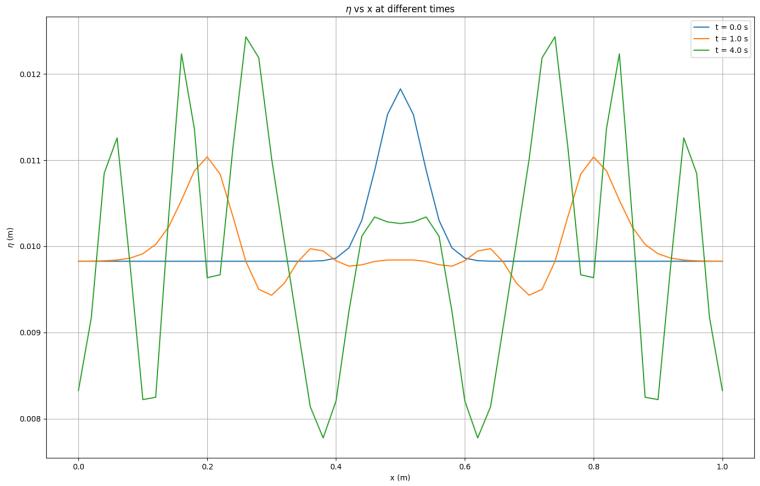


Figure 6: Evolution of the free surface elevation $\eta(x,t)$ over time $(t = 0.0, t = 1.0, t = 4.0 seconds)$. The initial Gaussian disturbance spreads outward, generating waves, but numerical instabilities apparent as oscillations at later times.

The plot shows the progression of $\eta(x,t)$ at the specified times. Initially $t = 0.0\,\mathrm{s}$, the Gaussian peak is symmetric and centered at $x = 0.5\,\mathrm{m}$, reflecting the initial condition. At $t = 1.0\,\mathrm{s}$, the disturbance begins to propagate outward, spreading as waves. At $t = 4.0\,\mathrm{s}$, significant oscillations develop throughout the domain.

The initial Gaussian perturbation evolves into outward-moving waves, consistent with the physics of shallow water dynamics. The spread of the disturbance suggests propagation due to gravitational acceleration. At $t = 4.0\,\mathrm{s}$, the solution exhibits oscillatory noise, especially near the wave fronts. These artifacts highlight the instability of the FTCS scheme, a known limitation when applied to hyperbolic PDEs. While the qualitative behavior aligns with shallow water dynamics, the FTCS scheme's instability limits the accuracy of long-term solutions.

## 3. Waves with Burger's Equation

Finally, we explore nonlinear wave phenomena by studying the inviscid Burger's equation, a fundamental PDE that models wave propagation where the wave speed depends on the amplitude. The equation is:

$$\frac{\partial u}{\partial t} + u\frac{\partial u}{\partial x} = 0$$

,

or in flux-conservative form:

$$\frac{\partial u}{\partial t} + \frac{\partial}{\partial x}\left(\frac{u^2}{2}\right) = 0$$

.

Due to the nonlinear nature and potential for wave steepening leading to shock formation, standard numerical methods like the FTCS scheme can be unstable. To address this, we employ the leapfrog method, which offers improved stability for wave equations.

The leapfrog update formula for the inviscid Burger's equation is:

$u_j^{n+1} = u_j^{n-1} - \frac{\beta}{2}\left[(u_{j+1}^n)^2 - (u_{j-1}^n)^2\right]$, where $\beta = \dfrac{\Delta t}{\Delta x}$, $n$ denotes the time step, and $j$ denotes the spatial grid point. Implementing this method, we will simulate the evolution of an initial sine wave: $u(x,0) = \sin(x)$, with boundary conditions $u(0,t) = 0$ and $u(L_x,t) = 0$, where $L_x = 2\pi$. We will observe how the disturbance changes over time, analyzing the behavior of nonlinear waves and the effectiveness of the leapfrog method in handling numerical challenges associated with such simulations.

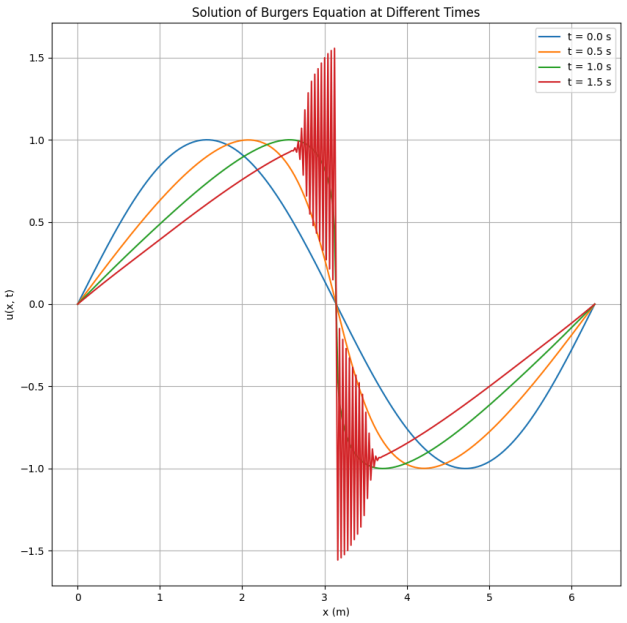


Figure 7:Evolution of the solution to the inviscid Burger's equation at $t = 0.0\,\mathrm{s}$, $t = 0.5\,\mathrm{s}$, $t = 1.0\,\mathrm{s}$, and $t = 1.5\,\mathrm{s}$, showing wave steepening due to nonlinearity and numerical oscillations near the forming shock.

The plot shows the evolution of the solution to the inviscid Burger's equation with an initial sine wave disturbance, $u(x,0) = \sin(x)$, using the leapfrog method. As time progresses, the wave steepens due to the nonlinear nature of the equation, where higher amplitudes propagate faster than lower ones. This steepening effect is evident in the plot, with the wave's leading edge becoming increasingly sharp as $t$ increases. By $t = 1.5\,\mathrm{s}$, the steep gradient near $x \approx 3.0$ indicates the onset of a shock-like structure, a characteristic feature of nonlinear wave dynamics. These oscillations are likely due to the leapfrog method, which, while stable for linear problems, can struggle with capturing shocks in nonlinear equations like the Burger's equation without additional stabilization techniques. The boundary conditions at $u(0,t) = 0$ and $u(L_x,t) = 0$ are satisfied, as the solution remains anchored at zero at both ends of the domain.

The observed wave steepening aligns with the theoretical behavior of the inviscid Burger's equation, demonstrating the method's ability to capture essential dynamics. However, the unrealistic oscillations near the shock reduce the solution's physical accuracy. These issues suggest that more advanced shock-capturing schemes, such as upwind methods or flux limiters, may be necessary for higher fidelity results.